

Supporting Informations - Computational analysis on native and extrinsic point defects in YAG using the metaGGA SCAN method

William Lafargue-Dit-Hauret¹, Mathieu Allix², Bruno
Viana³, Stéphane Jobic^{1*} and Camille Latouche^{1*}

¹Nantes Université, CNRS, Institut des Matériaux de Nantes
Jean Rouxel, IMN, F-44000, Nantes, France.

²Conditions Extrêmes et Matériaux: Haute Température et
Irradiation, CEMHTI, UPR 3079, CNRS, Université Orléans,
Orléans, 45071, France.

³PSL Research University Chimie ParisTech, IRCP, CNRS, Paris,
75005, France.

*Corresponding author(s). E-mail(s): stephane.jobic@cnrs-imn.fr;
camille.latouche@cnrs-imn.fr;

Contents

1	Corrections to the Defect Formation Enthalpies	3
1.1	Band-edges shift correction	3
1.2	Perturbated Host State correction	4
1.3	Potential alignment correction	5
1.4	Moss-Burstein correction	5
1.5	Makov-Payne correction	6
2	Calculation of defect concentrations	7
3	Intrinsic point defects	9
3.1	Stability phase domain	9
3.2	Initial position of interstitials	11
4	Ce-doping	13
5	Cr-doping	17

1 Corrections to the Defect Formation Enthalpies

Different post-treatment corrections were applied during the estimation of defect formation enthalpies (DFEs). In our investigations, the following corrections were taken into account:

- Band-edges shift (BS)
- Perturbated Host State (PHS)
- Potential Alignment (PA)
- Moss-Burstein (MB)
- Makov-Payne (MP)

1.1 Band-edges shift correction

Semi-local functionals are well-known to severely underestimate the band gap. Regarding the SCAN method, the gap value slightly increases due to the introduction of a kinetic term but still remains below the experimental measurements [1, 2]. To ensure a proper description, one of the most commonly encountered approach consists in performing an accurate calculation by the use of hybrid functionals or many-body methods on the fully relaxed SCAN structure.

During our investigations, we corrected the SCAN band gap with the one extracted from a PBE0 calculation (rigid shift). As evidenced in [Figure S1](#), the PBE06 band gap was found to be 6.90 eV. In this situation, the band-edges correction correspond to the shift of the SCAN Valence Band Maximum (VBM) $\Delta E_V = 1.17$ eV and the one of the Conduction Band Minimum (CBM) $\Delta E_C = 0.65$ eV. For the DFEs, the contribution of the BS correction is written as:

$$\Delta E_{BS} = q \times \Delta E_V \quad (1)$$

where q is the charge state of the defect.

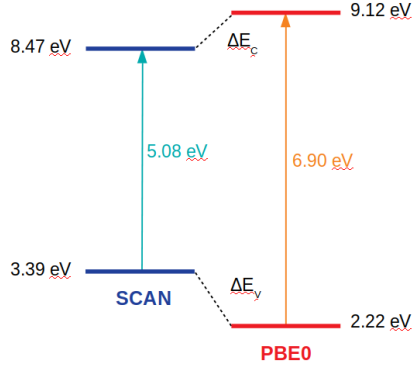


Fig. 1 Comparison of the band edges for SCAN and PBE0 calculations performed on the fully relaxed SCAN structure. ΔE_V and ΔE_C label shifts for the VBM and CBM, respectively.

1.2 Perturbed Host State correction

The creation of a defect in an host material affect the native electronic band structure by introducing localised states also called defect localized states (DLSs). When such states are lying just above or below the CBM (shallow defects), the electrons which occupy these DLSs tend to relax and stabilize within a perturbed host state (PHS). A similar situation arises for holes when DLS were found close to the VBM.

In the case where the band-edges have been shifted to more properly fit the experimental gap, a contribution to the DFEs is introduced due to the occupation of PHSs. The PHS correction expresses as:

$$\Delta E_{PHS} = z_e - \Delta E_C - z_h + \Delta E_V \quad (2)$$

where z_{e-} and z_{h+} are the number of electrons and holes occupying PHSs.

1.3 Potential alignment correction

The introduction of a net charge q into a neutral system induces an unidentified shift of energy levels. In such a case, the VBM of the charged faulted system should be aligned to the one of the host material, corresponding to the Potential alignment correction. This term is described in the following equation:

$$\Delta E_{PA} = q \times \overline{\Delta V} \quad (3)$$

where $\overline{\Delta V}$ corresponds to the average of the potential felt by atoms beyond a specific distance of the point defect.

1.4 Moss-Burstein correction

For small sizes of supercell, a Moss-Burstein-like effect appears due to the presence of PHSs. Thus, the contribution of band-filling effects need to be removed for shallow defects. For the electrons, the MB correction is formulated as:

$$\Delta E_{MB}^{e-} = - \sum^{n,k} \omega_k \eta_{n,k} (\epsilon_{n,k} - [E_C^{host} + \overline{\Delta V}]) \cdot \Theta (\epsilon_{n,k} - [E_C^{host} + \overline{\Delta V}]) \quad (4)$$

and for the holes as:

$$\Delta E_{MB}^{h+} = - \sum^{n,k} \omega_k (2 - \eta_{n,k}) ([E_V^{host} + \overline{\Delta V}] - \epsilon_{n,k}) \cdot \Theta ([E_V^{host} + \overline{\Delta V}] - \epsilon_{n,k}) \quad (5)$$

6 CONTENTS

where ω_k is the weight of k -point k , $\eta_{n,k}$ is the occupation of band n for k -point k , $\epsilon_{n,k}$ is the energy of band n for k -point k , and Θ is the Heaviside function.

1.5 Makov-Payne correction

For a given charged point defect, its replicated images due to periodic boundary conditions introduce spurious electrostatic contributions to the DFEs. Lany and Zunger proposed a general term to remove them [3]:

$$\Delta E_{MP} = (1 + c_{sh} (1 - \epsilon^{-1})) \frac{q^2 \alpha_M}{2\epsilon \Omega^{1/3}} \quad (6)$$

where c_{sh} is a geometry dependent correction term, ϵ is the dielectric constant of the material, α_M is the Madelung constant and Ω the volume.

We evaluated the isotropic electronic contribution for the primitive cell of the YAG material. We obtained $\epsilon_\infty = 3.36$ eV, in great agreement with the experimental value of 3.65 reported in Ref 4. Thus, for computational savings, we confidently took the experimental static dielectric constant [4].

2 Calculation of defect concentrations

The evolution of defects concentrations were determined depending on the synthesis conditions. To do so, we expressed the total concentration n_D of a defect D in a charge state q through Boltzmann statistics:

$$n_{D,q}(\mu_{E_F}) = N_D \cdot \exp\left(-\frac{\Delta_f H^{D,q}(E_F^{gr})}{k_B T_{gr}}\right) \quad (7)$$

where N_D is the number of accessible sites for the defect D , E_F^{gr} is the Fermi level at the growth temperature T_{gr} , k_B is the Boltzmann constant. The concentration of each defect can be accessed once E_F^{gr} is known. This quantity was obtained by solving iteratively the charge neutrality equation which ensures the total charge of the doped material is zero. This equation expresses as:

$$-n_e(E_F^{gr}) + n_h(E_F^{gr}) + \sum_D \sum_{q_i \in q_D} q_i \cdot n_{D,q_i}(E_F^{gr}) = 0 \quad (8)$$

where n_e corresponds to the concentration of free electrons in the conduction band:

$$n_e(E_F) = \int_{E_C}^{+\infty} g_e(E) f_{FD}(E - E_F) dE \quad (9)$$

and n_h the concentrations of free holes in the valence band:

$$n_h(E_F) = \int_{-\infty}^{E_V} g_h(E) (1 - f_{FD}(E - E_F)) dE \quad (10)$$

Both quantities depend on the Fermi-Dirac function $f_{FD}(E - E_F)$ and the 3D density of states of electrons $g_e(E)$ and holes $g_h(E)$. The computation of densities of states requires the knowledge of charge carrier effective masses. Here, the effective masses of electrons m_e^* and holes m_h^* are determined by

8 CONTENTS

fitting the curvature of the conduction band minimum (CBM) and valence band maximum (VBM) with the well-known parabolic function:

$$E(\mathbf{k}) = \frac{\hbar^2 \mathbf{k}^2}{2m^*} \quad (11)$$

We extracted the effective masses of holes and electrons from the fitting of the electronic bandstructure. The electronic gap is Γ -direct, as initially shown by Xu *et al.* [5]. using an LCAO method. We found $m_e^* = 1.138$ and $m_h^* = 3.271$, which will be used to determine the concentrations in electrons and holes, respectively.

3 Intrinsic point defects

3.1 Stability phase domain

Table 1 List of competitive phases. The ICSD number and space group symmetry of the structure before relaxations are provided.

Compound	ICSD number	Space group (number)
O ₂ molecule	-	P1 (1)
Y	660002	P63/mmc (194)
Al	43423	Fm-3m (225)
Al ₂ O ₃	73724	R-3c (167)
YAl ₃	58220	P63/mmc (194)
YAl ₂	609638	Fd-3m (227)
YAl	58209	Cmcm (63)
Y ₃ Al ₂	58215	P42/mnm (136)
Y ₂ Al	58211	Pnma (62)
Y ₂ O ₃	66242	Ia-3 (206)
Y ₄ Al ₂ O ₉	252973	P21/c (14)

The stability region presents a polygonial shape with five corner boundaries detailed in SI. One may distinguish i) two O-rich limits at the A (Y₂O₃/O_{2(g)}) and B (O_{2(g)}/Al₂O₃) points, and ii) three O-poor limits at the C (YAl₃/Al₂O₃), D (YAl₂/YAl₃) and E (Y₂O₃/YAl₂) points. Herein, we focused the following of our investigations on the A, B, C and E extreme synthesis conditions, assuming D and E atmospheres are similar.

Table 2 Extreme synthesis condition limits in terms of chemical potentials of Y, Al and O (in eV). The related deviations are given also, together with the corresponding competitive phases.

Point	μ_Y ($\Delta\mu_Y$)	μ_{Al} ($\Delta\mu_{Al}$)	μ_O ($\Delta\mu_O$)	Competitive phases
A	-37.99 (-10.13)	-16.72 (-8.99)	-6.02 (0.0)	Y ₂ O ₃ /O _{2(g)}
B	-38.35 (-10.50)	-16.50 (-8.77)	-6.02 (0.0)	O _{2(g)} /Al ₂ O ₃
C	-29.62 (-1.76)	-7.77 (-0.04)	-11.84 (-5.82)	YAl ₃ /Al ₂ O ₃
D	-29.27 (-1.41)	-7.88 (-0.15)	-11.88 (-5.86)	YAl ₂ /YAl ₃
E	-29.19 (-1.33)	-7.92 (-0.19)	-11.86 (-5.87)	Y ₂ O ₃ /YAl ₂

Table 3 Extreme synthesis condition limits in terms of chemical potentials of Y_2O_3 , Al_2O_3 and $\text{O}_{2(\text{g})}$ (in eV). The related deviations are given also, together with the corresponding competitive phases.

Point	$\mu_{\text{Y}_2\text{O}_3}$ ($\Delta\mu_{\text{Y}_2\text{O}_3}$)	$\mu_{\text{Al}_2\text{O}_3}$ ($\Delta\mu_{\text{Al}_2\text{O}_3}$)	μ_{O_2} ($\Delta\mu_{\text{O}_2}$)	Competitive phases
A	-94.04 (0.0)	-51.50 (-0.44)	-12.04 (0.0)	$\text{Y}_2\text{O}_3/\text{O}_{2(\text{g})}$
B	-94.77 (-0.73)	-51.07 (0.0)	-12.04 (0.0)	$\text{O}_{2(\text{g})}/\text{Al}_2\text{O}_3$
C	-94.77 (-0.73)	-51.07 (0.0)	-23.69 (-11.65)	$\text{YAl}_3/\text{Al}_2\text{O}_3$
D	-94.18 (-0.15)	-51.42 (-0.35)	-23.77 (-11.73)	$\text{YAl}_2/\text{YAl}_3$
E	-94.04 (0.0)	-51.50 (-0.44)	-23.77 (-11.73)	$\text{Y}_2\text{O}_3/\text{YAl}_2$

3.2 Initial position of interstitials

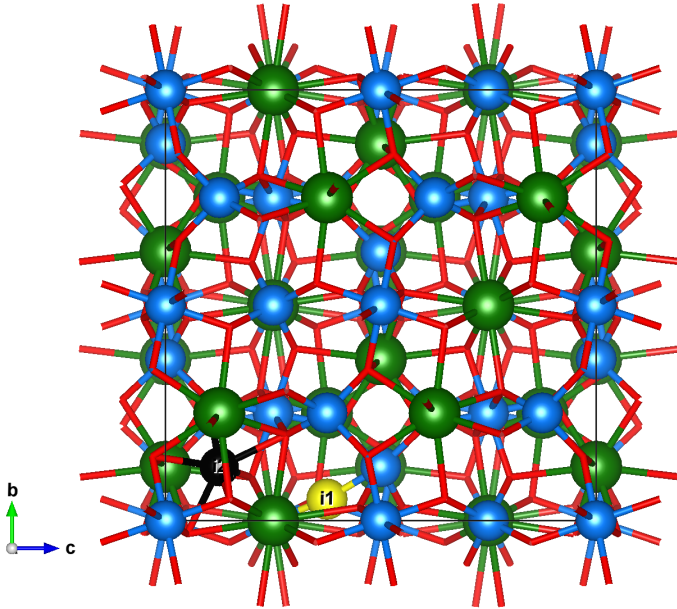


Fig. 2 Initial location of interstitial species. Anions are inserted in $48g$ site (yellow sphere) at $x = (0.125, 0.700, 0.550)$ and cations in $16b$ site (black sphere) at $x = (0.125, 0.125, 0.125)$.

12 CONTENTS

Table 4 List of charge transition levels for intrinsic species. Values are given respect to the VBM, and the bandgap is calculated at 6.90 eV.

Defect	$\epsilon(q/q')$	Value (eV)
Al_i	+3/+2	5.18
Al_i	+2/+1	5.47
Al_i	+1/0	5.74
Al_Y	0/-1	6.66
Al_Y	-1/-2	7.64
$V_{Al(T_d)}$	0/-1	1.96
$V_{Al(T_d)}$	-1/-3	2.54
$V_{Al(O_h)}$	0/-2	1.76
$V_{Al(O_h)}$	-2/-3	2.34
O_i	0/-1	2.52
O_i	-1/-2	3.53
V_O	+2/+1	3.85
V_O	+1/0	4.27
V_Y	0/-1	1.49
V_Y	-1/-2	2.01
V_Y	-2/-3	2.52
$Y_{Al(O_h)}$	+1/0	-0.13
$Y_{Al(O_h)}$	0/-1	7.09
$Y_{Al(T_d)}$	+1/0	-0.09
$Y_{Al(T_d)}$	0/-1	7.07
Y_i	+3/+2	4.71
Y_i	+2/+1	5.07
Y_i	+1/0	5.35

Table 5 Defect concentrations (in cm^{-3}) for intrinsic species at $T_{gr} = 1850$ °C under different synthesis conditions.

Defect	A	B	C	E	F
Al_i	3.4×10^{-1}	2.1×10^0	1.1×10^9	4.6×10^8	3.1×10^1
Al_Y	2.6×10^{14}	6.3×10^{15}	6.3×10^{15}	2.6×10^{14}	1.3×10^{15}
$V_{Al(T_d)}$	1.4×10^{14}	2.3×10^{13}	4.5×10^4	1.1×10^5	1.6×10^{12}
$V_{Al(O_h)}$	4.5×10^{12}	7.2×10^{11}	1.4×10^3	3.3×10^3	5.0×10^{10}
O_i	9.3×10^{14}	7.8×10^{14}	6.9×10^6	5.5×10^6	4.9×10^{11}
V_O	2.1×10^{12}	3.2×10^{12}	2.1×10^{19}	2.6×10^{19}	2.8×10^{13}
V_Y	1.1×10^{14}	4.2×10^{14}	8.3×10^5	8.0×10^4	5.9×10^{12}
$Y_{Al(O_h)}$	2.2×10^{19}	9.1×10^{17}	9.1×10^{17}	2.2×10^{19}	4.4×10^{18}
$Y_{Al(T_d)}$	2.8×10^{16}	1.2×10^{15}	1.2×10^{15}	2.8×10^{16}	5.7×10^{15}
Y_i	5.8×10^{-8}	1.5×10^{-8}	7.5×10^0	7.7×10^1	1.1×10^{-6}

4 Ce-doping

Table 6 List of competitive phases involving Ce. The ICSD number and space group symmetry of the structure before relaxations are provided.

Compound	ICSD number	Space group (number)
Ce	52843	Fm-3m (225)
Al ₂ Ce	606362	Fd-3m (227)
Al ₃ Ce	150603	P63/mmc (194)
AlCe	57551	Cmcm (63)
AlCe ₃	108788	Pm-3m (221)
Ce ₂ O ₃	621711	Ia-3 (206)
CeO ₂	61595	Fm-3m (225)
Ce ₇ O ₁₂	88755	R-3 (148)
CeAlO ₃	150277	I4/mcm (140)

Table 7 Extreme synthesis condition limits when YAG doped by Ce in terms of chemical potentials and the related deviations computed in eV, together with the corresponding competitive phases are reported. No Hubbard correction.

Point	μ_Y ($\Delta\mu_Y$)	μ_{Al} ($\Delta\mu_{Al}$)	μ_O ($\Delta\mu_O$)	μ_{Ce} ($\Delta\mu_{Ce}$)	Competitive phases
A'	-37.99 (-10.13)	-16.72 (-8.99)	-6.02 (0.00)	-56.46 (-11.84)	O ₂ /Y ₂ O ₃ /CeO ₂
B'	-38.35 (-10.50)	-16.50 (-8.77)	-6.02 (0.00)	-56.46 (-11.84)	O ₂ /Al ₂ O ₃ /CeO ₂
C'	-29.62 (-1.76)	-7.77 (-0.04)	-11.84 (-5.82)	-46.24 (-1.63)	YAl ₃ /Al ₂ O ₃ /CeAl ₃
D'	-29.27 (-1.41)	-7.88 (-0.15)	-11.88 (-5.86)	-45.89 (-1.28)	YAl ₃ /YAl ₂ /CeAl ₃
E'	-29.19 (-1.33)	-7.92 (-0.19)	-11.89 (-5.87)	-45.78 (-1.16)	YAl ₂ /Y ₂ O ₃ /CeAl ₃
F'	-29.25 (-1.39)	-7.98 (-0.25)	-11.85 (-5.83)	-45.61 (-0.99)	Y ₂ O ₃ /CeAl ₂ /CeAl ₃
G'	-29.35 (-1.49)	-8.08 (-0.35)	-11.78 (-5.76)	-45.41 (-0.79)	Y ₂ O ₃ /CeAl ₂ /Ce ₇ O ₁₂
H'	-31.84 (-3.98)	-10.57 (-2.84)	-10.12 (-4.10)	-48.26 (-3.64)	Y ₂ O ₃ /CeO ₂ /Ce ₇ O ₁₂
I'	-29.81 (-1.96)	-7.96 (-0.23)	-11.71 (-5.69)	-45.66 (-1.05)	Al ₂ O ₃ /CeAl ₃ /AlCeO ₃
J'	-32.20 (-4.35)	-10.35 (-2.62)	-10.12 (-4.10)	-48.26 (-3.64)	Al ₂ O ₃ /CeO ₂ /Ce ₇ O ₁₂
K'	-30.79 (-2.94)	-8.94 (-1.21)	-11.06 (-5.04)	-46.65 (-2.03)	Al ₂ O ₃ /Ce ₇ O ₁₂ /AlCeO ₃
L'	-29.73 (-1.88)	-7.98 (-0.25)	-11.73 (-5.71)	-45.61 (-0.99)	CeAl ₂ /CeAl ₃ /AlCeO ₃
M'	-29.51 (-1.65)	-8.05 (-0.32)	-11.75 (-5.73)	-45.46 (-0.84)	CeAl ₂ /Ce ₇ O ₁₂ /AlCeO ₃

14 CONTENTS

Table 8 Extreme synthesis condition limits when YAG doped by Ce in terms of chemical potentials and the related deviations computed in eV, together with the corresponding competitive phases are reported. $U_{eff} = 2$ eV.

Atm.	μ_Y ($\Delta\mu_Y$)	μ_{Al} ($\Delta\mu_{Al}$)	μ_O ($\Delta\mu_O$)	μ_{Ce} ($\Delta\mu_{Ce}$)	Competitive phases
A'	-37.99 (-10.13)	-16.72 (-8.99)	-6.02 (0.00)	-55.67 (-11.77)	O ₂ /Y ₂ O ₃ /CeO ₂
B'	-38.35 (-10.50)	-16.50 (-8.77)	-6.02 (0.00)	-55.67 (-11.77)	O ₂ /Al ₂ O ₃ /CeO ₂
C'	-29.62 (-1.76)	-7.77 (-0.04)	-11.84 (-5.82)	-45.24 (-1.34)	YAl ₃ /Al ₂ O ₃ /CeAl ₂
D'	-29.27 (-1.41)	-7.88 (-0.15)	-11.88 (-5.86)	-45.01 (-1.11)	YAl ₃ /YAl ₂ /CeAl ₂
E'	-29.19 (-1.33)	-7.92 (-0.19)	-11.89 (-5.87)	-44.93 (-1.03)	YAl ₂ /Y ₂ O ₃ /CeAl ₂
F'	-29.27 (-1.42)	-8.01 (-0.27)	-11.83 (-5.81)	-44.77 (-0.87)	Y ₂ O ₃ /CeAl ₂ /Ce ₂ O ₃
G'	-32.30 (-4.45)	-11.03 (-3.30)	-9.81 (-3.79)	-48.08 (-4.18)	Y ₂ O ₃ /CeO ₂ /Ce ₇ O ₁₂
H'	-30.29 (-2.43)	-9.02 (-1.29)	-11.15 (-5.13)	-45.78 (-1.88)	Y ₂ O ₃ /Ce ₇ O ₁₂ /Ce ₂ O ₃
I'	-29.78 (-1.92)	-7.93 (-0.20)	-11.74 (-5.72)	-44.92 (-1.02)	Al ₂ O ₃ /CeAl ₂ /AlCeO ₃
J'	-32.66 (-4.81)	-10.81 (-3.08)	-9.81 (-3.79)	-48.08 (-4.18)	Al ₂ O ₃ /CeO ₂ /Ce ₇ O ₁₂
K'	-30.77 (-2.91)	-8.92 (-1.18)	-11.08 (-5.06)	-45.91 (-2.01)	Al ₂ O ₃ /Ce ₇ O ₁₂ /AlCeO ₃
L'	-29.74 (-1.89)	-7.94 (-0.21)	-11.74 (-5.72)	-44.90 (-1.00)	CeAl ₂ /Ce ₂ O ₃ /AlCeO ₃
M'	-30.62 (-2.77)	-8.82 (-1.09)	-11.15 (-5.13)	-45.78 (-1.88)	Ce ₇ O ₁₂ /Ce ₂ O ₃ /AlCeO ₃

Table 9 Extreme synthesis condition limits when YAG doped by Ce in terms of chemical potentials and the related deviations computed in eV, together with the corresponding competitive phases are reported. $U_{eff} = 3$ eV.

Atm.	μ_Y ($\Delta\mu_Y$)	μ_{Al} ($\Delta\mu_{Al}$)	μ_O ($\Delta\mu_O$)	μ_{Ce} ($\Delta\mu_{Ce}$)	Competitive phases
A'	-37.99 (-10.13)	-16.72 (-8.99)	-6.02 (-0.00)	-55.31 (-11.51)	O ₂ /Y ₂ O ₃ /CeO ₂
B'	-38.35 (-10.50)	-16.50 (-8.77)	-6.02 (-0.00)	-55.31 (-11.51)	O ₂ /Al ₂ O ₃ /CeO ₂
C'	-29.62 (-1.76)	-7.77 (-0.04)	-11.84 (-5.82)	-44.91 (-1.11)	YAl ₃ /Al ₂ O ₃ /CeAl ₂
D'	-29.27 (-1.41)	-7.88 (-0.15)	-11.88 (-5.86)	-44.67 (-0.87)	YAl ₃ /YAl ₂ /CeAl ₂
E'	-29.19 (-1.33)	-7.92 (-0.19)	-11.89 (-5.87)	-44.59 (-0.79)	YAl ₂ /Y ₂ O ₃ /CeAl ₂
F'	-29.21 (-1.35)	-7.94 (-0.21)	-11.88 (-5.86)	-44.56 (-0.76)	Y ₂ O ₃ /CeAl ₂ /Ce ₂ O ₃
G'	-32.63 (-4.78)	-11.36 (-3.63)	-9.59 (-3.57)	-48.16 (-4.36)	Y ₂ O ₃ /CeO ₂ /Ce ₇ O ₁₂
H'	-31.41 (-3.56)	-10.15 (-2.41)	-10.40 (-4.38)	-46.77 (-2.97)	Y ₂ O ₃ /Ce ₇ O ₁₂ /Ce ₂ O ₃
I'	-29.72 (-1.86)	-7.87 (-0.13)	-11.78 (-5.76)	-44.71 (-0.91)	Al ₂ O ₃ /CeAl ₂ /Ce ₂ O ₃
J'	-32.99 (-5.14)	-11.15 (-3.41)	-9.59 (-3.57)	-48.16 (-4.36)	Al ₂ O ₃ /CeO ₂ /Ce ₇ O ₁₂
K'	-31.78 (-3.92)	-9.93 (-2.20)	-10.40 (-4.38)	-46.77 (-2.97)	Al ₂ O ₃ /Ce ₇ O ₁₂ /Ce ₂ O ₃

Table 10 Extreme synthesis condition limits when YAG doped by Ce in terms of chemical potentials and the related deviations computed in eV, together with the corresponding competitive phases are reported. $U_{eff} = 4$ eV.

Atm.	μ_Y ($\Delta\mu_Y$)	μ_{Al} ($\Delta\mu_{Al}$)	μ_O ($\Delta\mu_O$)	μ_{Ce} ($\Delta\mu_{Ce}$)	Competitive phases
A'	-37.99 (-10.13)	-16.72 (-8.99)	-6.02 (-0.00)	-54.97 (-12.02)	O ₂ /Y ₂ O ₃ /CeO ₂
B'	-38.35 (-10.50)	-16.50 (-8.77)	-6.02 (0.00)	-54.97 (-12.02)	O ₂ /Al ₂ O ₃ /CeO ₂
C'	-29.62 (-1.76)	-7.77 (-0.04)	-11.84 (-5.82)	-45.35 (-2.41)	YAl ₃ /Al ₂ O ₃ /CeAl ₃
D'	-29.27 (-1.41)	-7.88 (-0.15)	-11.88 (-5.86)	-45.00 (-2.06)	YAl ₃ /YAl ₂ /CeAl ₃
E'	-29.19 (-1.33)	-7.92 (-0.19)	-11.89 (-5.87)	-44.88 (-1.94)	YAl ₂ /Y ₂ O ₃ /CeAl ₃
F'	-29.30 (-1.45)	-8.04 (-0.30)	-11.81 (-5.79)	-44.54 (-1.60)	Y ₂ O ₃ /CeAl ₃ /Ce ₂ O ₃
G'	-32.96 (-5.11)	-11.70 (-3.96)	-9.37 (-3.35)	-48.27 (-5.32)	Y ₂ O ₃ /CeO ₂ /Ce ₇ O ₁₂
H'	-32.53 (-4.68)	-11.27 (-3.54)	-9.66 (-3.64)	-47.78 (-4.83)	Y ₂ O ₃ /Ce ₇ O ₁₂ /Ce ₂ O ₃
I'	-29.83 (-1.98)	-7.98 (-0.25)	-11.70 (-5.68)	-44.71 (-1.77)	Al ₂ O ₃ /CeAl ₃ /Ce ₂ O ₃
J'	-33.33 (-5.47)	-11.48 (-3.75)	-9.37 (-3.35)	-48.27 (-5.32)	Al ₂ O ₃ /CeO ₂ /Ce ₇ O ₁₂
K'	-32.90 (-5.04)	-11.05 (-3.32)	-9.66 (-3.64)	-47.78 (-4.83)	Al ₂ O ₃ /Ce ₇ O ₁₂ /Ce ₂ O ₃

Table 11 Extreme synthesis condition limits when YAG doped by Ce in terms of chemical potentials and the related deviations computed in eV, together with the corresponding competitive phases are reported. U_{eff} is set to 5 eV.

Atm.	μ_Y ($\Delta\mu_Y$)	μ_{Al} ($\Delta\mu_{Al}$)	μ_O ($\Delta\mu_O$)	μ_{Ce} ($\Delta\mu_{Ce}$)	Competitive phases
A'	-37.99 (-10.13)	-16.72 (-8.99)	-6.02 (-0.00)	-54.65 (-12.04)	O ₂ /Y ₂ O ₃ /CeO ₂
B'	-38.35 (-10.50)	-16.50 (-8.77)	-6.02 (-0.00)	-54.65 (-12.04)	O ₂ /Al ₂ O ₃ /CeO ₂
C'	-29.62 (-1.76)	-7.77 (-0.04)	-11.84 (-5.82)	-44.44 (-1.83)	YAl ₃ /Al ₂ O ₃ /CeAl ₃
D'	-29.27 (-1.41)	-7.88 (-0.15)	-11.88 (-5.86)	-44.34 (-1.72)	YAl ₃ /YAl ₂ /Ce ₂ O ₃
E'	-29.19 (-1.33)	-7.92 (-0.19)	-11.89 (-5.87)	-44.33 (-1.72)	YAl ₂ /Y ₂ O ₃ /Ce ₂ O ₃
F'	-29.57 (-1.71)	-7.78 (-0.05)	-11.85 (-5.83)	-44.39 (-1.77)	YAl ₃ /CeAl ₃ /Ce ₂ O ₃
G'	-33.43 (-5.58)	-12.16 (-4.43)	-9.06 (-3.04)	-48.57 (-5.96)	Y ₂ O ₃ /CeO ₂ /Ce ₂ O ₃
H'	-29.63 (-1.77)	-7.78 (-0.05)	-11.84 (-5.82)	-44.41 (-1.79)	Al ₂ O ₃ /CeAl ₃ /Ce ₂ O ₃
I'	-33.79 (-5.94)	-11.95 (-4.21)	-9.06 (-3.04)	-48.57 (-5.96)	Al ₂ O ₃ /CeO ₂ /Ce ₂ O ₃

Table 12 List of charge transition levels for extrinsic Ce species. Values are given respect to the VBM, and the bandgap is calculated at 6.90 eV.

Defect	$\epsilon(q/q')$	Value (eV)
$Ce_{Al}(O_h)$	+1/0	4.65 eV
$Ce_{Al}(O_h) \ U_{eff} = 2 \ eV$	+1/0	4.32
$Ce_{Al}(O_h) \ U_{eff} = 3 \ eV$	+1/0	4.12
$Ce_{Al}(O_h) \ U_{eff} = 4 \ eV$	+1/0	3.92
$Ce_{Al}(O_h) \ U_{eff} = 5 \ eV$	+1/0	3.71
Ce_Y	+1/0	4.28
$Ce_Y \ U_{eff} = 2 \ eV$	+1/0	3.84
$Ce_Y \ U_{eff} = 3 \ eV$	+1/0	3.65
$Ce_Y \ U_{eff} = 4 \ eV$	+1/0	3.66
$Ce_Y \ U_{eff} = 5 \ eV$	+1/0	3.42

5 Cr-doping

Table 13 List of competitive phases involving Cr. The ICSD number and space group symmetry of the structure before relaxations are provided.

Compound	ICSD number	Space group (number)
Cr	625711	Im-3m (229)
AlCr ₂	606748	I4/mmm (139)
Cr ₂ O ₃	26791	R-3c (167)
Y ₂ AlCrO ₆	4619	P21/n (14)
YCr ₄ Al ₈	198555	I4/mmm (139)

Table 14 Extreme synthesis condition limits when YAG doped by Cr in terms of chemical potentials and the related deviations computed in eV, together with the corresponding competitive phases are reported.

Point	μ_Y ($\Delta\mu_Y$)	μ_{Al} ($\Delta\mu_{Al}$)	μ_O ($\Delta\mu_O$)	μ_{Cr} ($\Delta\mu_{Cr}$)	Competitive phases
A''	-37.99 (-10.13)	-16.72 (-8.99)	-6.02 (0.00)	-24.47 (-6.17)	O ₂ /Y ₂ O ₃ /AlCrY ₂ O ₆
B''	-38.35 (-10.50)	-16.50 (-8.77)	-6.02 (0.00)	-24.31 (-6.00)	O ₂ /Al ₂ O ₃ /Cr ₂ O ₃
C''	-29.62 (-1.76)	-7.77 (-0.04)	-11.84 (-5.82)	-18.80 (-0.49)	YAl ₃ /Al ₂ O ₃ /AlCr ₂
D''	-29.27 (-1.41)	-7.88 (-0.15)	-11.88 (-5.86)	-18.74 (-0.43)	YAl ₃ /YAl ₂ /AlCr ₂
E''	-29.19 (-1.33)	-7.92 (-0.19)	-11.89 (-5.87)	-18.72 (-0.41)	YAl ₂ /Y ₂ O ₃ /AlCr ₂
F''	-38.10 (-10.25)	-16.65 (-8.92)	-6.02 (0.00)	-24.31 (-6.00)	O ₂ /Cr ₂ O ₃ /AlCrY ₂ O ₆
G''	-30.02 (-2.16)	-8.75 (-1.02)	-11.33 (-5.31)	-18.31 (0.00)	Cr/Y ₂ O ₃ /AlCr ₂
H''	-31.82 (-3.97)	-10.56 (-2.82)	-10.13 (-4.11)	-18.31 (0.00)	Cr/Y ₂ O ₃ /AlCrY ₂ O ₆
I''	-32.35 (-4.49)	-10.50 (-2.77)	-10.02 (-4.00)	-18.31 (0.00)	Cr/Al ₂ O ₃ /Cr ₂ O ₃
J''	-30.60 (-2.75)	-8.75 (-1.02)	-11.19 (-5.17)	-18.31 (0.00)	Cr/Al ₂ O ₃ /AlCr ₂
K''	-32.10 (-4.25)	-10.65 (-2.92)	-10.02 (-4.00)	-18.31 (0.00)	Cr/Cr ₂ O ₃ /AlCrY ₂ O ₆

Table 15 List of charge transition levels for extrinsic Cr species. Values are given respect to the VBM, and the bandgap is calculated at 6.90 eV.

Defect	$\epsilon(q/q')$	Value (eV)
$Cr_{Al}(O_h)$	+1/0	2.61
$Cr_{Al}(O_h)$	0/-1	6.65
$Cr_{Al}(T_d)$	+1/0	3.79
$Cr_{Al}(T_d)$	0/-1	4.98

References

- [1] Yang, Z.-h., Peng, H., Sun, J., Perdew, J.P.: More realistic band gaps from meta-generalized gradient approximations: Only in a generalized Kohn-Sham scheme. *Physical Review B* **93**(20), 205205 (2016). <https://doi.org/10.1103/PhysRevB.93.205205>. Accessed 2020-03-24
- [2] Long, O.Y., Sai Gautam, G., Carter, E.A.: Evaluating optimal u for 3d transition-metal oxides within the SCAN+ u framework. *Physical Review Materials* **4**(4), 045401 (2020). <https://doi.org/10.1103/PhysRevMaterials.4.045401>. Accessed 2020-04-12
- [3] Lany, S., Zunger, A.: Accurate prediction of defect properties in density functional supercell calculations. *Modelling and Simulation in Materials Science and Engineering* **17**(8), 084002 (2009). <https://doi.org/10.1088/0965-0393/17/8/084002>. Accessed 2020-02-20
- [4] Xu, R., Xu, Y.: *Modern Inorganic Synthetic Chemistry*. Elsevier, ??? (2017)
- [5] Xu, Y.-N., Ching, W.Y.: Electronic structure of yttrium aluminum garnet $\text{Y}_3\text{Al}_5\text{O}_{12}$. *Physical Review B* **59**(16), 10530–10535 (1999). <https://doi.org/10.1103/PhysRevB.59.10530>. Accessed 2020-02-10